ORIGINAL PAPER

The 2021 seismic hazard model for Slovenia (SHMS21): overview and results

Barbara Šket Motnikar[1] · **Polona Zupančič[1]** · **Mladen Živčić[1]** · **Jure Atanackov[2]** ·
Petra Jamšek Rupnik[2] · **Martina Čarman[1]** · **Laurentiu Danciu[3]** · **Andrej Gosar[1]**

Abstract

Slovenia is an earthquake-prone country with a moderate seismic hazard, characterized by relatively long recurrence intervals for strong earthquakes. With newly compiled data and revised info on active faults of the region, we are now able to supplement and enhance the probabilistic seismic hazard assessment, which was previously based mainly on the seismic catalog. The core of the seismic hazard model is the seismogenic source model combining various seismogenic representations i.e. area and gridded sources, and active faults. The ground motion model is characterized by a backbone model with regionalized parameters, which was also used to update the European seismic hazard model. We considered epistemic uncertainty in the most influential input parameters, implemented in a logic tree with 1377 branches. Considering the existing and forthcoming requests of the seismic design standard—Eurocode 8, we have developed the peak ground acceleration map of Slovenia and spectral acceleration maps for ten spectral periods, as well as seismic hazard curves and spectra for selected locations. The highest peak ground acceleration values (0.325 g) are at the western border of Slovenia with Italy. Other high-hazard areas extend across the Dinarides, in southeast Slovenia, and around the capital Ljubljana.

Keywords Probabilistic seismic hazard assessment · Slovenia · Seismogenic source models · Peak ground acceleration · Spectral accelerations · Logic tree

1 Introduction

Slovenia is an earthquake-prone country with low to moderate seismicity. The estimated moment magnitudes Mw of historical earthquakes are up to 6.5 and hypocenters are rather shallow, within the upper crust down to approximately 20 km. The current official ground shaking hazard map of Slovenia (ARSO 2001; Lapajne et al. 2003) is shown in Fig. S1

✉ Barbara Šket Motnikar
   barbara.sket-motnikar@gov.si

1   Slovenian Environment Agency (ARSO), Ljubljana, Slovenia

2   Geological Survey of Slovenia (GeoZS), Ljubljana, Slovenia

3   Swiss Seismological Service, ETH Zurich, Zurich, Switzerland

in the electronic supplementary material (ESM). It was prepared in 2001, in accordance with the Eurocode 8 (EC8) (CEN 2004) recommendations, by which the design ground acceleration is estimated in terms of the reference peak ground acceleration (PGA) on type A ground (according to EC8 classification) for the return period of 475 years. The highest values are in the central, NW, and SE parts of the country, while the hazard towards the NE and SW is rapidly decreasing. In 2005, Slovenia accepted EC8 as Slovenian standard and prepared its National Annex and since 2008, the National Annex specifications are law enforcement for seismic design in Slovenia.

Twenty years after the development of the current seismic hazard map, significant new data, models, methods, and knowledge have become available. The new findings require not only an update but a completely new development of the Slovenian seismic hazard model. Hereinafter, we will address the official hazard map, and the corresponding model as "previous", and label the models and results of this study as "new". Over the last seven years, the Slovenian Environment Agency (ARSO) and the Geological Survey of Slovenia (GeoZS) have been working together to develop a new national seismic hazard model.

For the first time in Slovenia, we established a database of active faults, complete with the corresponding seismotectonic parameterization (Atanackov et al. 2021a), which is one of the important features of the new seismic hazard model. Several active fault systems developed in the contact zone between Adriatic and European plates. Reverse faults prevail at the contact between Adria Foreland and Dinarides and in the Italian part of the Southern Alps, and regional strike-slip faults prevail in the Dinarides and the southeastern Alps in Slovenia (Fig. 1).
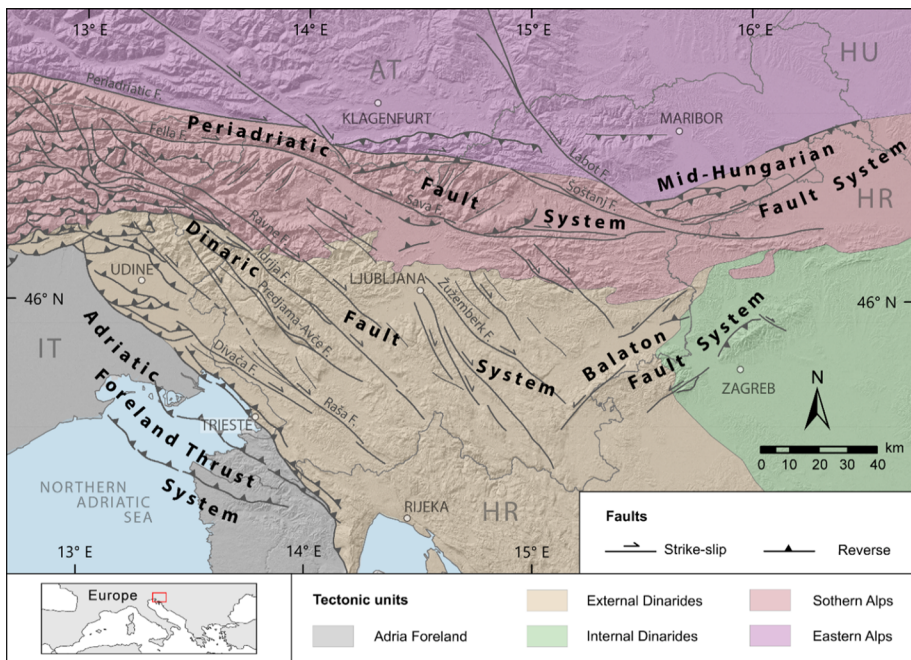
Fig. 1 Tectonic units [simplified from Schmid et al. (2020)) and active faults (summarized after Atanackov et al. (2021a) and Poli and Zanferrari (2018)] in the study area—Slovenia, and parts of Italy (IT), Austria (AT), Hungary (HU), and Croatia (HR)

Besides the development of the fault source model from the database of active faults, an area source model and a smoothed seismicity model were also considered. The structure of the described seismogenic source models together with the corresponding logic tree represents the core of the first part of this study. In detail, it addresses the estimation of the parameters that determine the magnitude-frequency distribution (MFD), which includes the slope of the function curve, the maximum possible magnitude (i.e. Mmax), and the annual rate of earthquakes above a threshold magnitude, which are systematically evaluated for each seismogenic source model. Determination of other parameters of seismogenic sources (e.g., fault type, focal mechanism, slip rate) is described in Atanackov et al. (2021a, b). The seismic source geometry and parameterization files are available in Pangaea online repository (Atanackov et al. 2022). Please see the Excel tables FS_PSHA and AS_PSHA for fault and area seismic source parameters, respectively, as well as FS_PSHA_Help and AS_PSHA_Help for their description.

In the second part, we present and discuss the results of the new probabilistic seismic hazard assessment (PSHA). The forthcoming EC8 is expected to replace the most fundamental parameter PGA with two spectral acceleration (SA) parameters, namely at the spectral period of 1 s, and at the spectral period that determines the plateau of the elastic response spectrum (CEN 2021). Therefore, besides the PGA map, the new PSHA provides also SA maps for 10 spectral periods. Results in terms of seismic hazard curves and spectra for selected locations in Slovenia are also presented.

2 Methodology of the Key components of SHMS21

2.1 PSHA main features

The previous and the new seismic hazard maps of Slovenia resulted from a probabilistic framework (Cornell 1968), which calculates the ground shaking hazard considering all possible earthquakes that could affect the study area. The approach was described in four steps by e.g. Reiter (1990): (1) delineation and parametrization of all possible seismogenic sources in the influential area; (2) determination of the MFD at each seismogenic source; (3) choice of the ground motion model (GMM) describing how ground motion values decrease with distance; and (4) calculation of the probability of exceedance of the ground motion reference values.

By definition (e.g. Reiter 1990), the seismogenic sources represent structurally and seismically homogeneous areas. The main source of seismological data is an earthquake catalog, harmonized in the border region, and unified in terms of earthquake magnitude. The probabilistic approach assumes a Poissonian distribution of earthquakes in time and space, which means that all dependent events (foreshocks and aftershocks) are removed from the catalog. For the estimation of the annual seismicity rate, only the complete part of a declustered catalog is used.

Due to the comparatively limited available data and knowledge around the year 2000, the previous seismic hazard model was mainly based on historical seismological data, and a simplified seismotectonic model (Poljak et al. 2000). The seismogenic source model was based on spatially distributed seismic activity rates. The smoothing (Frankel 1995) approach was methodologically modified and adapted to Slovenian geological characteristics (Lapajne et al. 1997, 2000, 2003; Šket Motnikar et al. 2000), and implemented in OHAZ software (Zabukovec 2000). The chosen MFD function form was the same as for

the new model. The empirical ground motion model of Sabetta and Pugliese (1996) was used.

The methods used in the development of the new Slovenian seismic hazard model are described in the following sections. We begin with a description of the seismogenic source representation i.e. point, area, and fault source models. Point sources implement the gridded smoothing of observed seismicity, which is quite similar to the previous PSHA model, and rely mostly on seismological data. Area source model parametrization makes use of both, seismological, and geological data, while the fault sources are mostly based on geological data. Epistemic uncertainty and aleatory variability of input parameters are thoroughly addressed.

For the calculation of seismic hazard, we used the OpenQuake (OQ) software (Pagani et al. 2014; OpenQuake 2021), which has been validated under the PSHA code verification procedure performed by the Pacific Earthquake Engineering Research Center (Hale et al. 2018).

2.2　Earthquake catalog

Systematic collection of macroseismic data on the territory of Slovenia started after the great Ljubljana earthquake (epicentral intensity $I_0 =$ VIII-IX EMS-98) in 1895. A few years later, the first seismographs in the Austro-Hungarian monarchy were installed in Ljubljana (in 1897) and Trieste (in 1898) (Plešinger and Kozák 2003).

Following the Skopje, Northern Macedonia earthquake in 1963, a large project that studied seismicity, seismotectonics, and seismic hazard in the Balkan region was carried out in the early seventies. One of the major outcomes was the compilation of the first modern catalog of the region (Shebalin et al. 1974), compiled using the methodology developed within the European earthquake catalog project (Karnik 1971). The part for Slovenia was compiled by V. Ribarič and later published as the Catalogue of Earthquakes in Slovenia (Ribarič 1982). Most of the earthquake parameters were derived from macroseismic data. The reason is that Ljubljana station was the only station operating in Slovenia until 1975 (and even so with only a few years of operation between 1918 and 1958). The neighboring countries had very few stations as well, which was not sufficient to estimate hypocentral parameters from instrumental records.

The Ribarič (1982) catalog is the basis for the KPN2018 catalog (Živčić et al. 2018) used in this study. For recent years, it was supplemented by seismic bulletins of the Slovenian network and annual reports published regularly as Potresi v letu (PVL 1994–2019). To assess the seismic hazard in Slovenia it is necessary to evaluate the contributions also from the neighboring areas. For that reason, we supplemented the KPN2018 catalog to cover the area between 12° and 18.5° E and between 44° and 48° N. We used the most recent available catalogs of the neighboring countries ((ZAMG 2002) for Austria, (Zsíros et al. 1988) for Hungary, (GFZ 2008) for Croatia, and (Poli et al. 2002) for Friuli/Italy), and bulletins (NEIC 2015) and databases of the international seismological agencies (ISC 2021) as well as the most recent European SHARE (Stucchi et al. 2013) and Balkan area BSHAP catalogs (Markušić et al. 2016).

The target threshold magnitude for the KPN2018 catalog was set to local magnitude ML = 3.5, which is lower than the threshold for some of the input earthquake catalogs. To include smaller magnitude earthquakes than the input catalog threshold and to extend the time coverage past the most recent entry we used ISC and national bulletins

(GeoRisk 1995–2019 for Hungary, INOGS 1977–2014 for Friuli, ZAMG 2006–2014, and 1998–2013 for Austria).

2.2.1 Harmonization on borders and unification of moment magnitude

In compiling the final version of the KPN2018 catalog, we adopted the sovereignty principle according to which the best parameters for an earthquake are the ones determined by the authors from the country where the earthquake happened. The only exception was Bosnia and Herzegovina for which no recent catalog was available and we had to rely on BSHAP and Croatian earthquake catalogs as the nearest proxy. In the case of a "double" (conflicting) claim, the preferred location was the one with higher intensity reported or, in the case of a tie, the one from the most recent publication.

For use in PSHA applications, all earthquakes are described by moment magnitude Mw. Very few earthquakes and only that from the most recent period have Mw determined from the moment tensor inversion. For all the earthquakes in the KPN2018 catalog, we collected various size estimates (epicentral intensity I_0, magnitudes of various types: surface wave magnitude MS, body wave magnitude mb, local magnitude ML, surface wave magnitude from horizontal component MLH, duration magnitude MD). Due to a rather small number of Mw determinations, the number of earthquakes with both Mw and some other size estimate did not allow the derivation of reliable conversion relation to Mw. We rather searched the published relations derived on larger data sets in nearby geographic regions and tested them against our limited data set to apply the one with the best chi-squared score. The only exception is the relation between epicentral intensity I_0 and Mw that we derived for lower intensities (up to VI-VII EMS-98) using orthogonal regression on available data. The relations used for the conversion are given in Table S1 (in ESM).

2.2.2 Catalog declustering

Further requirement on the earthquake catalogs for the time-independent seismic hazard assessment is to use only independent events that follow a Poisson distribution. Removing dependent events (foreshocks and aftershocks) is a rather subjective task as there are no clear definitions of how to distinguish between independent and dependent events. Among numerous algorithms based on different assumptions, the Gardner and Knopoff (1974) windowing method is the most often used one. It assumes that an event that is within the time and space window of a stronger event is dependent. The size of the windows scales with the magnitude of the stronger event. The window sizes used for declustering KPN2018 are given in Table S2 (in ESM), and the declustered earthquake catalog is shown in Fig. 2.

2.2.3 Catalog completeness

We analyzed the completeness of the declustered earthquake catalog KPN2018 inside the influential area, which includes 1595 main shocks (Fig. 2). The majority of earthquakes in the catalog is from the pre-instrumental era, which enables only magnitude estimation from macroseismic data (Živčić 1994, 2004; Živčić et al. 2010, 2015). As a consequence, the frequency of earthquakes by magnitude classes strongly depends on the conversion from intensity I_0, using equation $Mw = 0.749 * I_0 + 0.022$ for I_0 up to VI-VII, and equation $Mw = 0.423 * I_0 + 2.182$ for larger I_0 (Živčić et al. 2015). Converted from the two equations, Mw magnitude values are not continuous, but one can obtain only values of 3.8, 4.1,
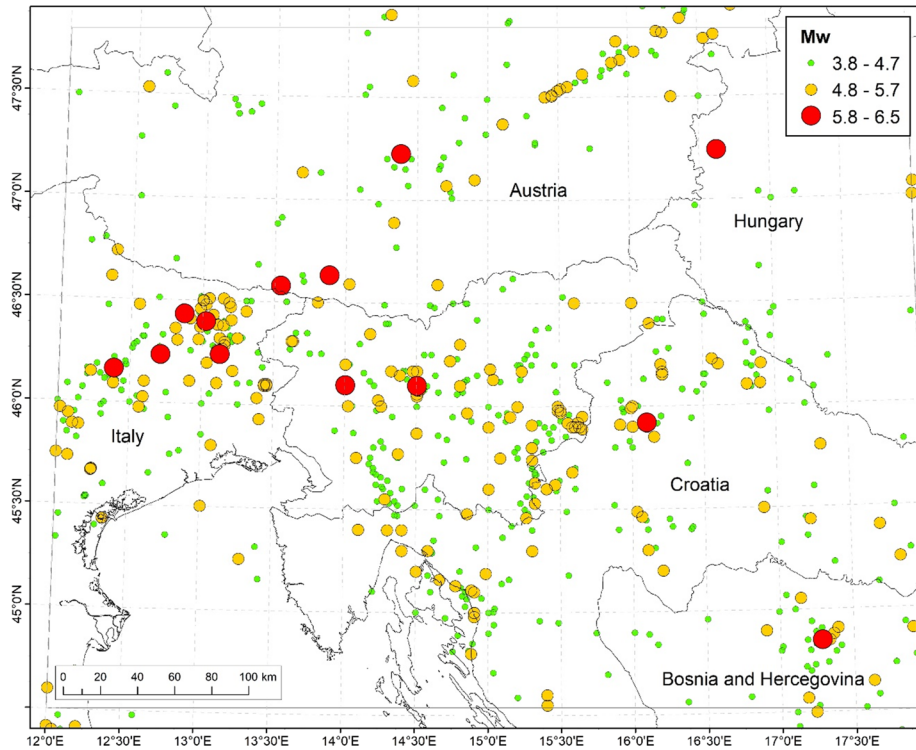
Fig. 2 Harmonized and declustered earthquake catalog from period 456 to 2018. Size and color of circles denote moment magnitude Mw

4.5, … that correspond to intensity V, V–VI, VI, … EMS-98, respectively. Therefore the completeness analysis only makes sense for these values of Mw.

The completeness period is estimated graphically by determining the most prominent change in gradient of the cumulative curve that shows the number of earthquakes in 10-year time intervals with $Mw \geq Mc$. For $Mc = 3.8$, we estimated the corresponding completeness year as 1875 (blue curve in Fig. 3), and the corresponding complete catalog is shown in Fig. 4.

Similarly, we analyzed the cumulative curves for Mw values that correspond to integer intensity values. As the recurrence interval of earthquakes increases with Mw, we accordingly increased the time interval (graphs for individual Mc are not shown). We estimated the completeness year for $Mc = 4.5$ (intensity VI), 5.1 (intensity VII), and 5.6 (intensity VIII) to be 1850, 1840, and 1570, respectively (Table 1).

Completeness analysis for Mw 5.6 and especially for larger magnitudes is unreliable due to a very small number of events. At first glance, approximately the same completeness period for various Mw up to 5.1 seems surprising (Fig. 3), but on the other hand, historical reasons set an important boundary in macroseismic investigations around 1880. Beginning with the Zagreb earthquake (9 November 1880, $Mw = 5.6$), a series of moderate and strong earthquakes occurred in the considered area until the Ljubljana earthquake in 1895 ($Mw = 5.8$), which encouraged authorities to order the systematic work on reporting, collecting, and analyzing earthquakes.
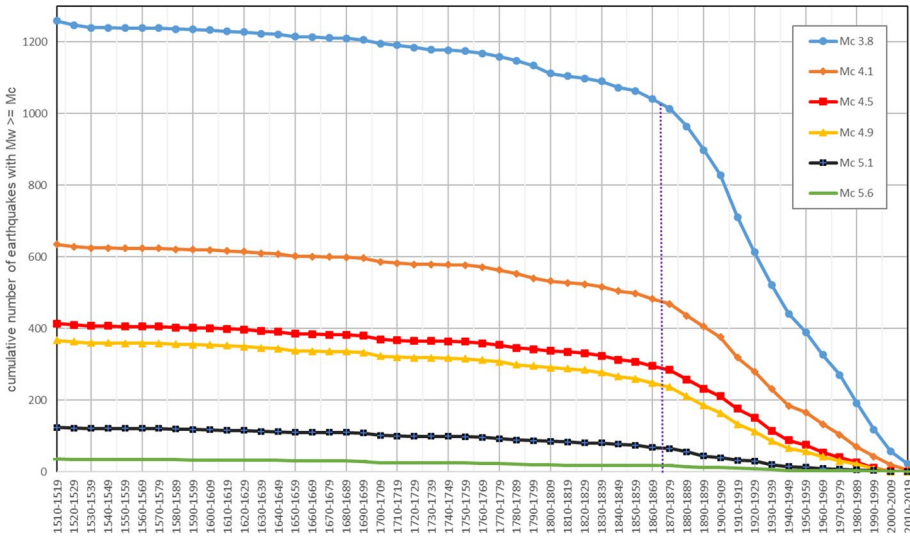
Fig. 3 Cumulative number of earthquakes with Mw ≥ Mc in 10-year time intervals end estimated start of the completeness period for Mc 3.8 (dot line). Curves for other Mc are added only to show the importance of a milestone in macroseismic practice in the late nineteenth century
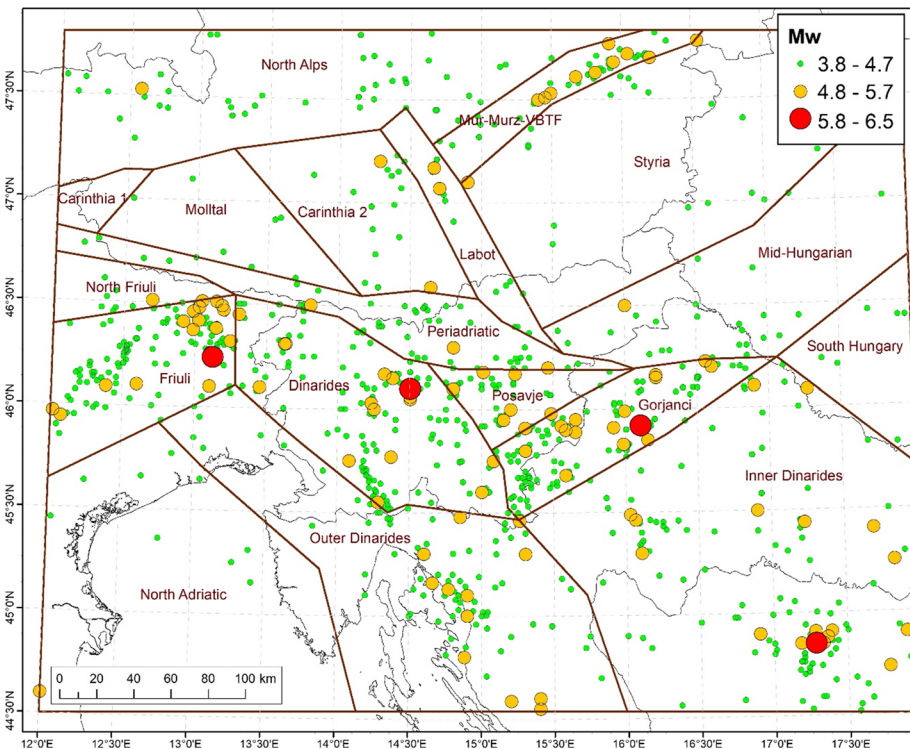
Fig. 4 Area (A) source model and earthquakes with Mw ≥ 3.8 from the complete catalog from 1875 onward

Table 1 Intensity value I_0, the corresponding completeness magnitude Mc, and completeness year for the declustered catalog KPN2018

I_0	Mc	Year of completeness
V	3.8	1875
VI	4.5	1850
VII	5.1	1840
VIII	5.6	1570

With the reorganization of macroseismic practice at that time, some work has been done more thoroughly also on damaging earthquakes from the recent past, which supports the estimated year of completeness 1875 for Mc = 3.8. This could explain, why there is only a slight difference in completeness year for stronger earthquakes.

Due to the almost identical completeness periods for Mw 3.8, 4.5, and 5.1, we decided to use only the complete catalog for Mw = 3.8, as it provides the largest number of events and therefore better determines activity rates in statistical terms. Also, a too-small number of earthquakes at larger magnitudes prevents us to determine reliable completeness periods for larger magnitudes. To overcome this, we consider the specific values of the magnitudes from the whole earthquake catalog by applying the energy-based model (Lapajne et al. 2003) in point seismic sources (See Sect. 2.3.7). We believe that this has successfully replaced the use of several complete earthquake catalogs.

2.3 Seismogenic source model: characterization

While the previous hazard map is based mostly on earthquake catalog, the new hazard model relies on all known seismotectonic, geological, and seismological data and knowledge. This is achieved by using three seismogenic source models: area sources (A model), grid point sources (P model), and combined fault & background sources (F + B model), where background considers all earthquakes below a magnitude threshold M_t. The models' weak and strong points, as well as our confidence in the model's credibility for future seismicity forecasting as a weight in hazard computation, are expressed in Table 2. In the continuation, we briefly explain each seismogenic source model and the methodology of the estimation of the parameters. The parameterization tables AS_PSHA and FS_PSHA for area and fault sources respectively, as well as shape files of their geometry, are provided in an online repository (Atanackov et al. 2022).

2.3.1 Area source model (A model)

Area zones are the most common type of seismogenic sources in PSHA (Danciu and Giardini 2015). For the delineation of the area sources, we gave priority to the presence of faults or fault systems with the potential to generate earthquakes with Mw ≥ M_t, in which geometric and kinematic structural trends are uniform or related. We decided to use this criterion, as we consider it to be more representative for modeling (future) seismicity than the information on past seismicity, mainly because of the relatively short period of earthquake catalog completeness, and because the presence of the faults might be an indicator of the future migration of seismicity along such structures. Furthermore, this may most

Table 2 Seismogenic source models advantages and weaknesses

Model	Weight	Advantages	Weakness
A	0.4	Combines tectonic characteristics (delineation is based mainly according to structural geologic and kinematic homogeneity) and seismological data (activity rate and Mmax are estimated from the earthquake catalog)	Not strictly homogeneous in observed seismicity; partly subjective in zone delineation and parameter estimation
P	0.4	Distributed seismicity is zoneless, which requires almost no subjective parameter estimation; the model corresponds to the lack of knowledge as only a few earthquakes in the catalog are proved to be generated by a specific fault	Some future earthquakes might occur outside areas of recorded seismicity; not appropriate for very long return periods
F + B	0.2	Modeling large earthquakes on faults, and small earthquake in the back-ground corresponds to our current knowledge and data	Poorly constrained source delineation and parametrization; significant slip rate and its seismic part uncertainty; some faults might be unknown

likely be true for area zones that consist of known large active faults, with the seismic moment being released in strong but infrequent earthquakes.

The model consists of 18 area source zones that cover the whole influential area (Fig. 4). We parameterized area source zones based on geological (geometry delineation, dip, strike, rake, seismogenic depth) and seismological (seismic activity rate, Mmax, seismogenic depth) data and knowledge, as we briefly describe in the next sections.

2.3.2 Point sources—smoothed seismicity model (P model)

We introduced the point source model P to consider the distributed seismicity. Point sources are centers of grid cells, which are set in the whole influence area of the hazard calculation. Cell dimensions are 10×10 km because a denser grid would overestimate the accuracy of the epicenter location from the non-instrumental period of the earthquake catalog. P model is zone-free and assumes that future earthquakes will occur in the vicinity of past earthquakes (historical approach). We applied two stages of the smoothing procedure. The first stage of smoothing is circular, which considers uncertainty in epicenter location. The second stage is fault-oriented elliptical smoothing, which is based on the presupposed directions of seismogenic faults in different tectonic regions (Lapajne et al. 2003). We estimated the parameters in each grid cell mostly from seismological data (seismic activity rate, Mmax, hypocentral depth) but we inherited some geological information (dip, strike, rake) from the A model.

2.3.3 Fault and background model (F + B model)

For the first time, we parameterized fault-specific seismogenic sources in Slovenia and its surroundings, which enables us to estimate the hazard also outside areas of observed past seismicity. However, as only large faults in Slovenia are known and parameterized, we have to combine seismogenic faults with background seismicity. Based on the assumption that a large majority of faults capable to generate earthquakes with $Mw \geq M_t$ is known and parameterized, we model the seismicity from M_t to Mmax on fault sources and the seismicity from Mmin to M_t in the background. We have defined background sources as area sources (A model), and as smoothed seismicity in grid cells (P model), in two equally weighted models F + A, and F + P.

A compilation of regional geologic characteristics, active faults capable of generating $Mw \geq 5.5$ earthquakes, and methodology of parametrization are described in detail by Atanackov et al. (2021a). Based on this study, we determined the fault-specific seismogenic sources, while some seismogenic faults fully outside the national border were compiled from DISS (DISS 2018) and SHARE (Basili et al. 2013) databases. We further critically evaluated the model of fault sources, to include only independent sources. Particularly, we evaluated their geometry and proximity to other sources. If surface traces of two fault sources are only a few kilometers apart, we merged them or retained only the dominant source. A seismogenic fault source is geometrically a 3D structure, which is described by fault trace, dip, and seismogenic depth. A fault buffer is a surface projection of a given fault source (Fig. 5). We have defined four categories of fault activity with the corresponding probability as follows (Atanackov et al. 2021b): active (1.0), probably active (0.7), potentially active (0.5), and questionably active (0.25). The final fault-specific source model consists of 89 fault sources, which we believe to be complete for $Mw \geq 5.8$ earthquakes. This is also the selected value of magnitude threshold M_t between fault and background sources.
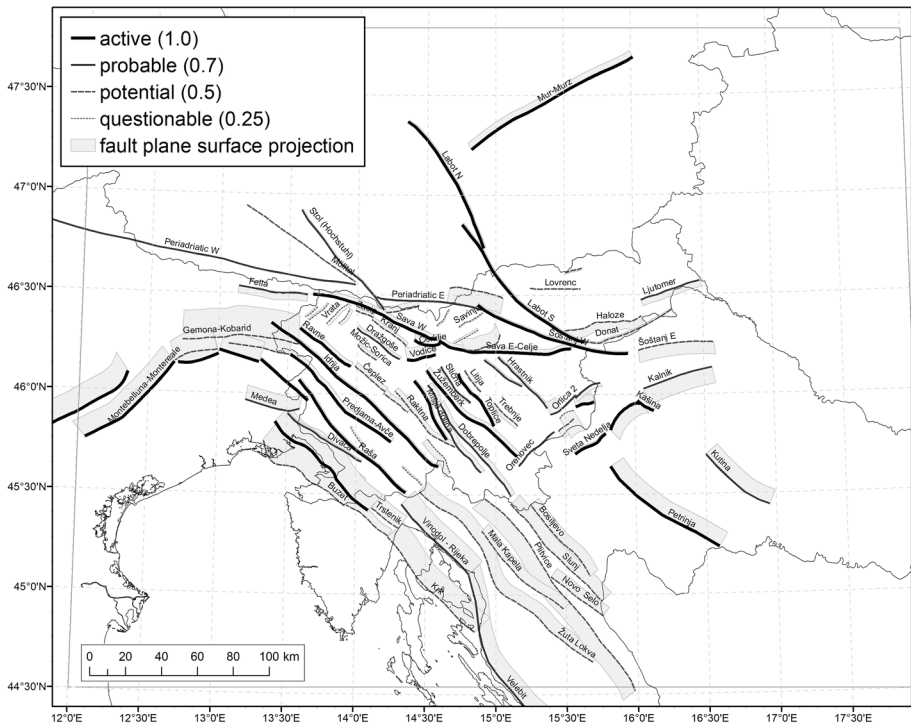
Fig. 5 Seismogenic fault (F) source model: fault traces and fault plane surface projections (fault buffers). The thickness of the fault trace shows the probability of fault activity with weights in parentheses

We estimated fault source parameters mostly from geologic and seismotectonic data, as we briefly describe in the continuation. A detailed description is given in Atanackov et al. (2021b). Only seismogenic depth and seismic coupling are partly determined using the seismological data.

2.3.4 Magnitude frequency distribution (MFD)

To describe the spatial and temporal seismic activity rates, we used a cumulative doubly truncated Gutenberg-Richter (GR) *magnitude frequency distribution,* defined by Cornell and Vanmarcke (1969):

$$N(m) = N(m_0) \frac{10^{-b(m-m_0)} - 10^{-b(m_u-m_0)}}{1 - 10^{-b(m_u-m_0)}} \quad (1)$$

where $N(m)$ is the cumulative number of earthquakes with a magnitude equal to or higher than m, the seismic activity rate $N(m_0)$ is the total number of earthquakes with a magnitude equal to or higher than the lower bound magnitude m_0, m_u is the upper bound magnitude, and b (or GR b-value) is the decay rate.

In our study, the given MFD is applied to the whole area of interest, and all seismogenic sources. The upper bound magnitude m_u equals the maximum possible magnitude (Mmax) of earthquakes in any given area. GR a-value is defined as a logarithm of annual $N(0)$.

Since the estimate of the b-value is dependent on earthquake catalog declustering, we tested the stability of the obtained b-values using different time and space window sizes. Estimated b-values using Aki's method (Aki 1965) range between 0.98 and 1.03 with a standard deviation of 0.03. Considering that the uncertainty of the individual magnitude estimates is 0.7 or larger for two-thirds of earthquakes, we adopted b = 1 as the preferred value for all seismogenic sources. To evaluate the seismic hazard, we have to consider the long-term average of the GR a- and b-values. Stable values can be obtained if the area and time span are large and with a sufficient number of earthquakes (e.g. Godano and Pingue 2000). Smaller datasets can be used providing that all magnitudes in the catalog were determined in the same manner, which is not the case for the catalogs used for PSHA, where Mw is derived by converting from various earthquake size estimates (e.g. Kagan 1999). We didn't consider epistemic uncertainty in the b-value, because the results of our sensitivity study show only negligible impact.

As described in Eq. 1, the parameters to be determined for MFD (besides the fixed b-value) are the maximum magnitude Mmax and annual rate of seismic activity or GR a-value. Their estimation approach depends on the seismogenic source geometry type (area, point, or fault source), and is described in detail in continuation.

2.3.5 Minimum magnitude Mmin

For national seismic hazard maps, the minimum magnitude *Mmin* of hazard calculation is typically between Mw 4.0 and 5.0. According to Bommer and Crowley (2017), Mmin should denote the lowest magnitude of an earthquake that is capable of generating damage of engineering interest. Therefore, Mmin depends on the purpose of the PSHA study; for the national hazard maps, Mmin should be lower than e.g. for nuclear power plants. The calculated ground motion values increase with lower Mmin, as GMMs give positive values even for very low magnitudes. Therefore, the purpose of Mmin is also to exclude contributions to the hazard arising from earthquakes causing no or negligible damage. As Mmin may significantly affect the ground motion estimates, the choice of Mmin is quite important.

According to the EC8 standard (CEN 2004), objectives of seismic design are the protection of human lives, damage limitation, and smooth operation of important structures, so its goal is not the prevention of small damage of intensity V or VI after European Macroseismic Scale 1998 EMS-98 (Grünthal 1998). In Slovenia, the seismicity is shallow, and small magnitude earthquakes can cause damage. The earthquake with the smallest instrumentally determined magnitude that caused moderate structural damage (of grade 3 on EMS-98) occurred on November 1, 2015. The estimates of its Mw range from 4.28 determined by USGS (2021) to 4.45 determined by INGV (2021). It hit two villages in the Gorjanci area with intensity VII EMS-98 (Šket Motnikar et al. 2016). Such relatively small, but damaging earthquakes should not be overlooked, so we chose Mw = 4.3 for Mmin.

2.3.6 Maximum magnitude Mmax

A model: The maximum observed moment magnitude in the whole earthquake catalog KPN2018 (Živčić et al. 2018) is 6.5, which occurred on 6 May 1976 in Friuli (Tertulliani et al. 2018; Finetti et al. 1979). The second-largest magnitude 6.4 was estimated for the Idrija earthquake on 26 March 1511 (Camassi et al. 2011; Košir and Cecic 2011). Besides, there are 6 earthquakes in the catalog with magnitudes between 6.0 and 6.2. For

the seismological assessment of Mmax, we defined five superzones that are based on seismotectonic characteristics and completely cover the influential area (Fig. S2 in ESM). We determined Mmax following the EPRI approach (Johnston et al. 1994; Wiemer et al. 2016), which is based on maximum observed magnitude and a priori Mmax distribution that is suitable in a given seismotectonic region. In our case, we chose normal distribution for European seismo-tectonically active regions (Ameri et al. 2015) with the mean value of 6.8 and sigma of 0.4 (yellow line in Fig. S3 in ESM). Secondly, we updated the prior distribution with a likelihood function *L(Mmax)*, which is based on the doubly truncated exponential frequency magnitude distribution with b-value = 1 (blue line in Fig. S3). Further, we implemented Kijko's correction (Kijko 2012), which turns out to be unnecessary because differences are negligible. Finally, the estimated Mmax is given in terms of the probability density function, which is continuous, so it should be discretized to a few Mmax values with the corresponding weights. For this purpose, we used the 3-point discretization method (Miller and Rice 1983). An example of this discretization and the results of Mmax estimation in all five superzones are shown in Fig. S4 and Table S3 (in ESM), respectively. Mmax estimates in each area source zone are inherited from the corresponding superzone.

P model: The maximum magnitude for the whole influential area is determined as the maximum observed value in the earthquake catalog (6.5) plus an increment. We chose three increment values with the corresponding weights in parentheses: 0.0 (0.2), 0.2 (0.5), and 0.4 (0.3), which are modeled as epistemic uncertainty of Mmax in the logic tree. The largest weight is given to the best estimate value of 6.7.

F model: We have calculated the maximum possible moment magnitudes using three empirical *magnitude scaling relationships* (MSR): Wells and Coppersmith (1994), Hanks and Bakun (2002), and Leonard (2010). For all three MSR, we have assumed a full-length rupture scenario, which is quite unlikely; in order not to be overly conservative in Mmax estimates, we used the mean relationship (and not e.g. mean + sigma). We consider the relationship with rupture length (RL) parameter for strike-slip faults and with rupture area (RA) parameter for dip-slip faults because we think RL and RA are more robust parameters for strike-slip and dip-slip faults, respectively.

2.3.7 Annual activity rate (GR a-value)

A model: We statistically determine the annual activity rate in each source zone, by counting the number of earthquakes from the complete catalog (Mc = 3.8, 1875). The GR a-value is the logarithm of the corresponding number of earthquakes above magnitude 0, as defined and used in OpenQuake (Pagani et al.2014).

P model: We determined the GR a-value with two approaches. In the first, all earthquakes from the complete catalog (Mc = 3.8, 1875) are circularly and elliptically smoothed and counted in each grid cell. In the second approach, we calculated the activity rate from the *energy-based* model that enables us to consider large historical earthquakes, not registered in a complete catalog due to their too short time span. This model considers estimated magnitude values of past earthquakes and consequently as such replaces the use of several complete earthquake catalogs (for different magnitude thresholds). As already described, we consider only one complete earthquake catalog, when characterizing the seismogenic potential of the region. Calculation details of the energy-based model are described in (Lapajne et al. 2003). Instead of earthquakes counting, we determine the activity rate using the relationship between magnitude and released seismic energy, which is further converted to the corresponding number of earthquakes. The energy-based model considers

the whole earthquake catalog from the year 456 onward. However, from the strongest historical earthquakes that influence hazard results in terms of the energy model, only the earthquakes near Idrija in 1511, Mw 6.4 (Camassi et al. 2011; Košir and Cecic 2011), and near Villach in 1348, Mw 6.2 (Caracciolo et al. 2021) are not in the complete catalog. Both earthquakes have been thoroughly investigated, and their effects have been recorded, so there is no doubt about their existence and the maximum intensity estimate is at least approximately adequate.

F model: For a fault-specific source, we estimate its annual activity rate using the Youngs and Coppersmith (1985) equation for converting the slip rate estimates. We have determined the minimum, maximum, and best estimates of slip rate, all as an expert opinion based on all available data, including geologic data (offset of lithologic markers, sediments), age dating, geomorphic data (offset of geomorphic markers), geophysical and geodetic data (GNNS, InSAR, leveling data, extensometer), as is described in (Atanackov et al. 2021a, b). We additionally estimated seismic coupling, the percentage of slip rate that is released as seismic activity. It was determined in two ways: with a fixed fraction of 70% (Ward 1998), and with a fault-specific seismic coupling ratio defined by Carafa et al. (2017). Exceptionally, for some seismogenic faults fully outside Slovenia, we adopted the parametrization from DISS (2018), including slip rates estimates, which are already adjusted for coupling ratio (present 100% coupling).

2.3.8 Other parameters of seismogenic sources

Besides the parameters of MFD, source parametrization requires also a determination of seismogenic (upper and lower) depth, focal mechanism (dip, strike, and rake), seismic coupling, and rupture aspect ratio. For most parameters, estimation is primarily done for fault sources and deduced for the corresponding area zones and point sources. Additionally, for area and point sources, the hypocentral depth has been determined as well. Estimation of all the above-mentioned parameters was based on published methodology and data, fieldwork, paleoseismic trenching, geomorphologic analyses, and interpretations of all available geophysical and seismological data (Atanackov et al. 2021b, 2022).

2.4 Ground motion model (GMM)

In the previous Slovenian seismic hazard map (Lapajne et al. 2003), the GMM of Sabetta and Pugliese (1996) was used because many accelerograms, used in the estimation of coefficients, were from the neighboring Friuli area. However, in the next decade, having available strong-motion data set from new seismic stations, and consequently new ground-motion prediction equations (Douglas 2021), it turned out that this GMM does not adequately fit new data, because of its small standard deviation and its non-zero bias (Bindi et al. 2009).

The sensitivity study on nine published GMMs was performed (Šket Motnikar 2010), with all other parameters remaining the same as for the previous hazard map. The choice of the nine GMMs was influenced by publications in peer-reviewed journals, experts' elicitation and recommendations, magnitude range, the proximity of used ground-motion data, and limitations of the software used. The results showed an approximately 30% increase in PGA values compared to values obtained in 2001 using Sabetta and Pugliese (1996) relations. It was also shown that GMM with magnitude-dependent sigma exaggerated the impact of low magnitudes and in turn the choice of minimum magnitude.

Nowadays, many new predictive ground-motion equations are available in different regions of the world (Douglas 2021). First, we intended to apply similar criteria for the selection of GMMs as in (Šket Motnikar 2010), putting forward the most often used GMM of Bindi et al. (2014, 2017), Akkar and Bommer (2010), Akkar et al. (2014a, b, 2014a), and Chiou and Youngs (2014). But contrary to the previous practice of using a set of GMMs, the scaled backbone concept has been introduced and increasingly used in the last years (Douglas 2018). A backbone model relies upon a reference model, for which the parameters are calibrated and their distribution is modeled in a logic tree. In such a way, a backbone model uncertainty is more apparent, in comparison to the case with a classical suite of GMMs.

Another advantage of a backbone model is that parameters might be regionally adapted, which is another reason to consider the same scaled backbone GMM (Weatherill et al. 2020; Kotha et al. 2020) that was used in the 2020 update of the European Seismic Hazard Model (ESHM20) (Danciu et al. 2021) for active shallow crust tectonic regime. In the final model of our choice (Weatherill et al. 2020), two parameters are region-dependent, namely a coefficient of attenuation (c3), which describes the attenuation rate, and a source scaling factor (L2L), which is related to a local stress regime at the source. The distribution of both parameters was determined region by region in five clusters (besides the default values, denoted as region 0). As recommended by the authors, the three-point discrete approximation to the Gaussian distribution is applied for both region-dependent parameters, resulting in 9 branches of the Slovenian logic tree. Actually, the source scaling factor node was replaced with the envelope of the source-scaling factor and statistical uncertainty that describes the within-model uncertainty of GMM. For the majority of magnitude and distance ranges, the source-scaling factor dominates (Weatherill et al. 2020).

The whole Slovenian territory (except three sites at the Hungarian border), and the majority of the surrounding influence area were classified in region 1, which denotes slow to average attenuation. The few remaining sites belong to region 0, denoting the default (European average) attenuation rate. A sensitivity study, comparing the described original regionalization with the case, where all sites are classified in region 1, shows no significant difference in the results. This is even more evident, when the area of hazard calculation consists only of the sites inside the Slovenian border, resulting in negligible difference. So for the final calculation, we classified all sites as region 1, and we set the grid of sites at 3×3 km.

Besides the constant regression coefficients, the seismic source parameters that enter the chosen GMM are magnitude Mw, distance R (in terms of RJB, the shortest distance from a site to the surface projection of the rupture plane), focal mechanism, hypocentral depth, and soil type (vs30 = 800 m/s in our case). In particular, the OQ input data for area and point sources contains also nodal plane parameters (strike, rake, dip) and hypocentral depth (including their aleatory variability), and the upper and lower seismogenic depth, which enables the calculation of the RJB distance based on the finite rupture settings. In this calculation, we have used a finite rupture model with OQ, as described in Monelli et al (2014).

2.5 Epistemic uncertainties: logic tree

Epistemic uncertainty of Slovenian PSHA is modeled through a logic tree, representing alternatives in seismogenic source models, in some most important source parameters, and parameters of GMM. The structure of the logic tree with 1377 branches is shown in Fig. 6.
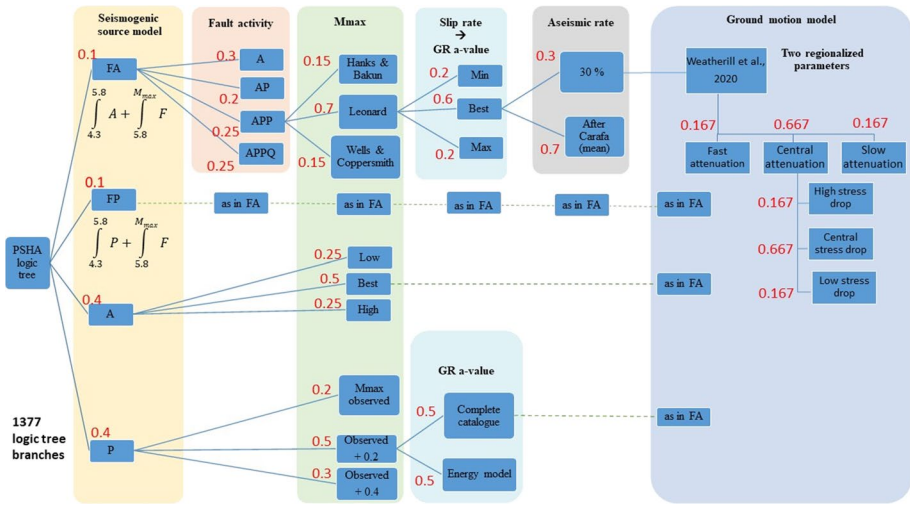
Fig. 6 Logic tree of the Slovenian PSHA model with 1377 branches

The core of the logic tree for hazard computation is represented by three seismogenic source models: A, P, and F + B models. Their weights 0.4, 0.4, and 0.2 respectively, have been determined by expert judgment according to Table 2. For the F + B model, there is a slight difference in the spatial distribution of PGA, depending on whether the background is represented with the area or with the point sources. As we do not have any reason to prefer one or another type of background, we decided that both options are considered with equal weights for F + A (0.1) and F + P (0.1) models.

In the seismogenic fault source model, we have defined logic tree branches that determine some most important parameters and their weights in parenthesis as follows:

– 4 logic tree branches according to the probability of fault activity: only active (A) faults (0.3); only active and probable (AP) faults (0.2); active, probable, and potential (APP) faults (0.25); and all (APPQ) faults (0.25);
– 3 values of slip rate; min (0.2), max (0.2) and best estimates (0.6);
– 2 values of aseismic ratio: fixed 30% aseismic ratio (0.3), and fault specific value calculated from (Carafa et al. 2017) (0.7);
– 3 values of Mmax based on MSR from Leonard (2010) (0.70), Wells and Coppersmith (1994) (0.15), and Hanks and Bakun (2002) (0.15).

In the A model, we have defined 3 Mmax estimates: low (0.25), best (0.5), and high (0.25), using the EPRI method and (Miller and Rice 1983) 3-point discretization approach.

The P model logic tree consists of:

– 3 values of Mmax: maximum observed value 6.5 plus an increment (0, 0.2, 0.4), defined as an expert opinion: 6.5 (0.2), 6.7 (0.5), 6.9 (0.3);
– 2 values of activity rate based on the complete catalog (0.5), or energy-based model (0.5).

As mentioned before, the chosen scaled backbone GMM of (Weatherill et al. 2020) has two regionally defined parameters (two nodes), for which 3-point discretization gives 9 logic tree branches:

– three values of attenuation coefficient, and
– three values of the envelope of source variability and statistical uncertainty.

Besides the logic tree, aleatory variability of the hazard model is considered in the ground motion model, but also in some other source parameters of A model: faulting style, strike, rake, dip, and hypocentral depth (Atanackov et al. 2022). As all the above area source parameters are inherited also to the corresponding point sources, the same aleatory variability is considered in smoothed seismicity (P) model.

3 Main results

Following Cornell (1968), and using the OpenQuake hazard library (Pagani et al. 2014; OpenQuake 2021) we have calculated the annual probability of exceedance of the reference intensity levels on rock (Vs30 = 800 m/s) in terms of PGA and SA. The main results consist of ground shaking hazard curves, uniform hazard spectra (UHS), and hazard maps for various return periods. The mean results represent weighted mean values according to the logic tree with 1377 end-branches from Fig. 6. Median and four percentiles (5th, 16th, 84th, 95th) values are calculated as well.

3.1 Results per seismogenic source models: ground shaking hazard maps

Ground shaking maps depicting PGA values for a mean return period of 475 years are presented in Fig. 7 for each seismogenic source models A, P, F + A, and F + P. The F + B models, namely F + A, and F + P consists of two parts, where the threshold magnitude $M_t = 5.8$ divides the contributions from the fault sources and the background. Their separate contributions are shown in Fig. 8 (for fault sources above M 5.8) and Fig. 9 (for background sources below magnitude 5.8; left: area sources, and right: point sources).

## 3.2 PGA seismic hazard map for the 475-year return period

The overall mean and median values of the PGA maps on rock (Vs30 = 800 m/s) for a 475-year return period, which combine four seismogenic source models, are shown in Fig. 10. The 5, 16, 84, and 95 percentile PGA maps are also calculated, and their values are compared in the Discussion and Conclusion section.

For designing earthquake-resistant buildings (as part of Slovenian legislation), we proposed the use of mean values, because they are sensitive to skewness, and consider all branches of the logic tree, including conservative values from fault seismic sources and energy-based models. The mean values are significantly higher than median values in western Slovenia, in the area from Bovec to Postojna. Mean values consider the important Dinaric fault system, and the location of the strongest historical earthquake in the Slovenian catalog, while using median values we would completely overlook them.

In analogy to the current official seismic hazard map, all values below 0.1 g are ascribed to 0.1 g, and all other calculated PGA values are rounded up in each PGA
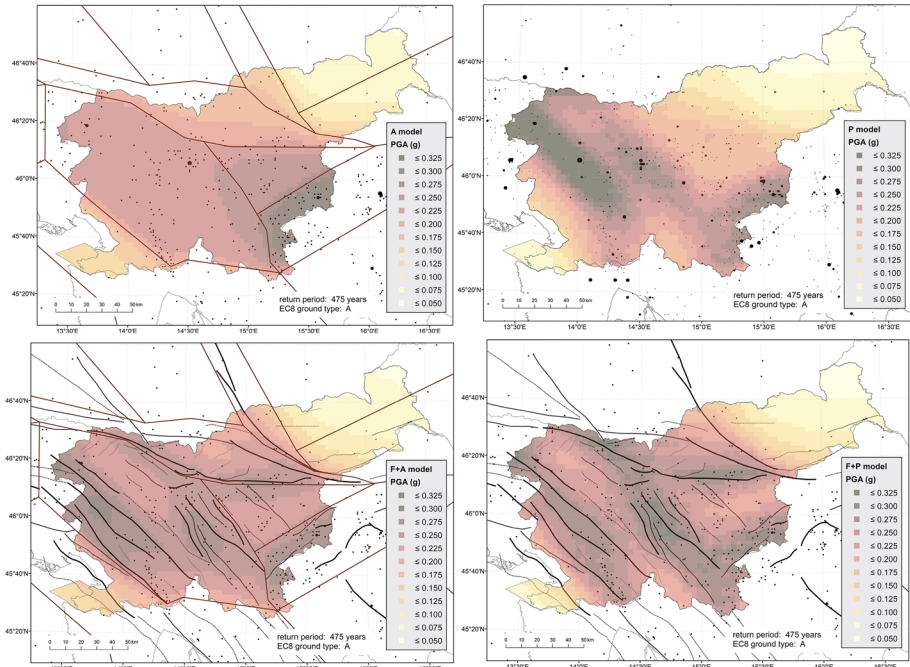
Fig. 7 Mean PGA maps of individual (A, P, F + A, F + P) seismogenic source models. Earthquakes from the whole KPN2018 catalog are shown on the map of the P model, while the other three maps are presented together with the corresponding source model and earthquakes from the complete KPN2018 from 1875. All hazard maps are estimated for a return period of 475 years and a reference Vs30 value of 800 m/s
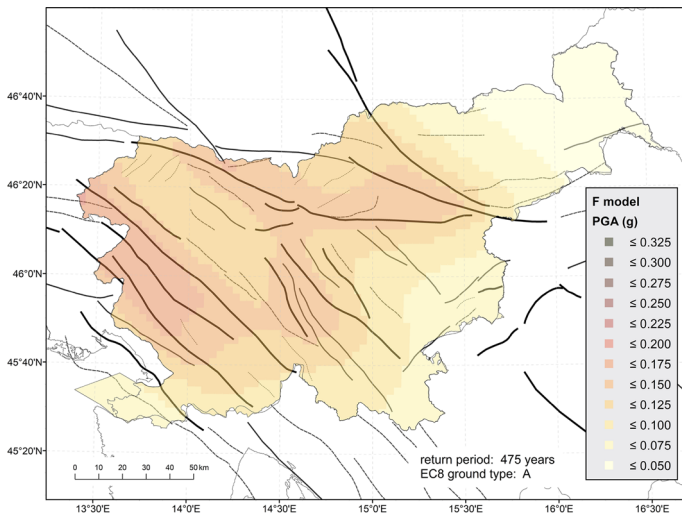
Fig. 8 Mean PGA map from fault-specific sources only (magnitude from 5.8 on) for a return period of 475 years and a reference Vs30 value of 800 m/s
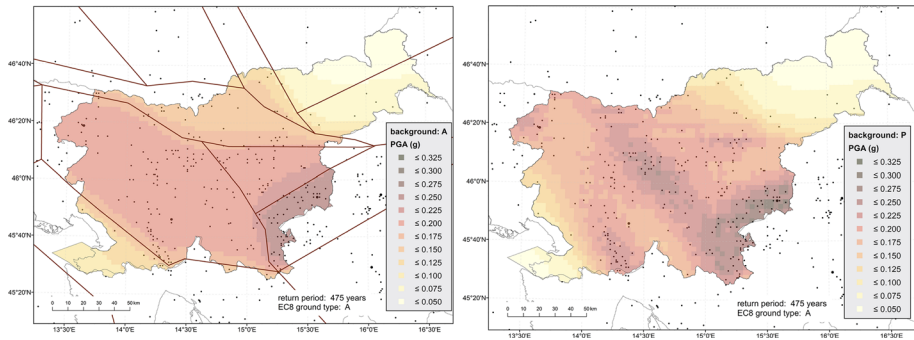
Fig. 9 Mean PGA map from background sources only: A sources (left) or P sources (right). In both cases, only a magnitude range from 4.3 to 5.8 is considered. Both hazard maps are estimated for a return period of 475 years and a reference Vs30 value of 800 m/s

class of width 0.025 g. The places on the isolines should be classified into a higher PGA class. It is proposed that the seismic hazard map from Fig. 11 replaces the current official design ground acceleration map, which is an appendix to the National Annex of EC8.

The new Slovenian seismic hazard map (Fig. 11) reaches the largest (rounded) mean PGA values (0.325 g) in a sparsely populated area at the western border with Italy, which is due to the highly active seismogenic sources in the Friuli region. The area of 0.3 g covers the region around Idrija (which coincides with the most important Dinaric faults and the strongest historical earthquakes), and the SE part of Slovenia (which is the area of the densest seismicity).

Fig. S5 (in ESM) shows the difference between the new (Fig. 11) and old (Fig. S1 in ESM) national seismic hazard maps. On both maps, the area of larger seismic hazard runs along the central part of Slovenia from the NW to the SE of the country and diminishes to the northeast and southwest. The old values are higher only around the Ptuj area. In the northern part of central Slovenia, in NE, and SW Slovenia, the hazard values on both maps are comparable. In the Dinarides and Gorjanci area source zones, and around Celje, the ground acceleration values are higher on the new map, with the largest increase near Črnomelj in the SE part of Slovenia, with the difference up to 0.125 g.

We compared the new Slovenian PGA hazard map also with the ESHM13 (Giardini et al. 2014; Woessner et al. 2015) (Fig. S6 in ESM) and ESHM20 (Danciu et al. 2021) (Fig. S7 in ESM) mean PGA maps within national borders. Calculated ESHM PGA values are not spatially interpolated. For comparison purposes, values are grouped into the same classes as on the new national map and shown at the class boundaries. The maximum values from ESHM13 (0.350 g) and ESHM20 (0.325 g) maps are very similar to Slovenian (0.325 g) and the largest hazard values are again spread from the NW to the SE of the country. However, both European maps peak near Brežice (SE of Slovenia), while the national hazard map has three equally high areas (0.3 g): beside Brežice, also areas around Bovec and Idrija, both in western Slovenia. The seismicity in this part of western Slovenia is relatively low, however, there are some most important seismogenic Dinaric faults, and in the Slovenian earthquake catalog, there is also the epicenter of the strongest (Mw 6.4) known Slovenian earthquake from 1511 (Camassi et al. 2011; Košir and Cecic 2011). The main reason for higher values in western Slovenia in the national hazard map arises from
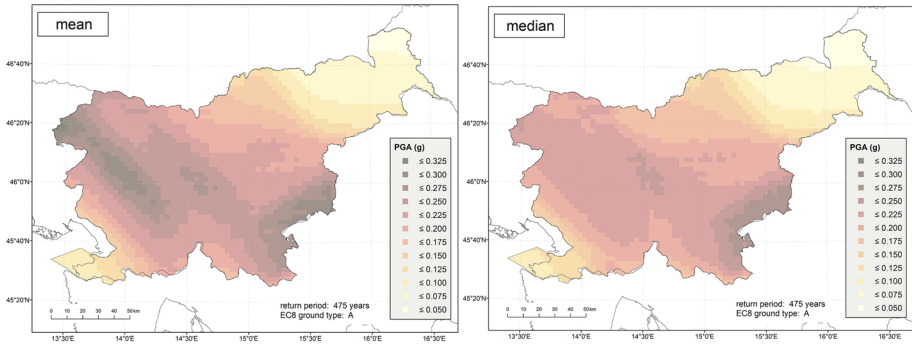
**Fig. 10** Mean (left) and median (right) PGA map on rock (Vs30 = 800 m/s) for a 475-year return period
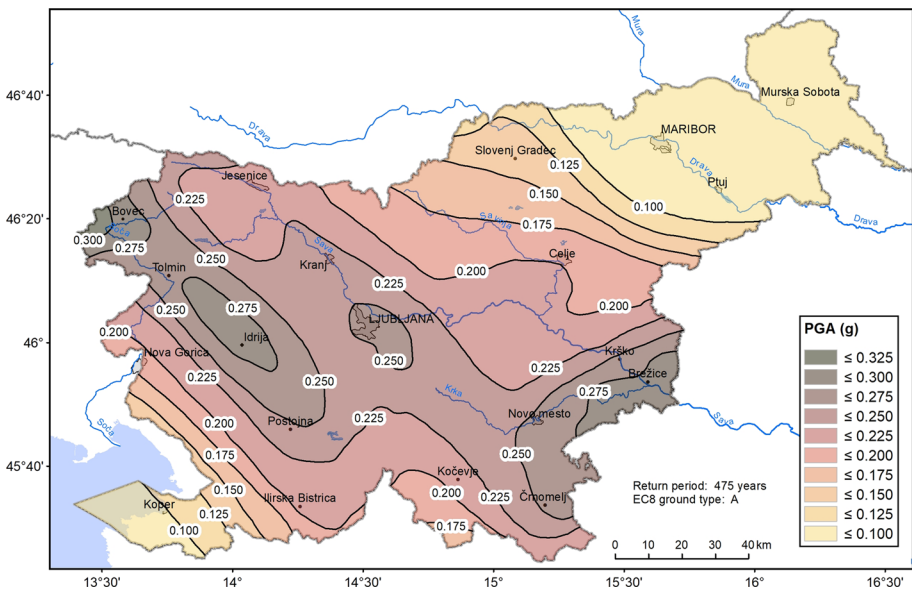
Fig. 11 New seismic hazard map of Slovenia (2021): proposed design ground acceleration on rock (Vs30 = 800 m/s) for a 475-year return period

the energy-based smoothing model, which is implemented only in the Slovenian seismic source model.

Here we focused on the hazard results for the 475-year return period, however, two hazard maps with return periods of 95 and 2475 years are shown in Figs. S8 and S9 in ESM, respectively.

3.3 Ground motion hazard curves for the selected locations

The 475-year return period is recommended for ordinary buildings and the "no-collapse" limit state requirement in modern seismic design standards i.e. EC8. The
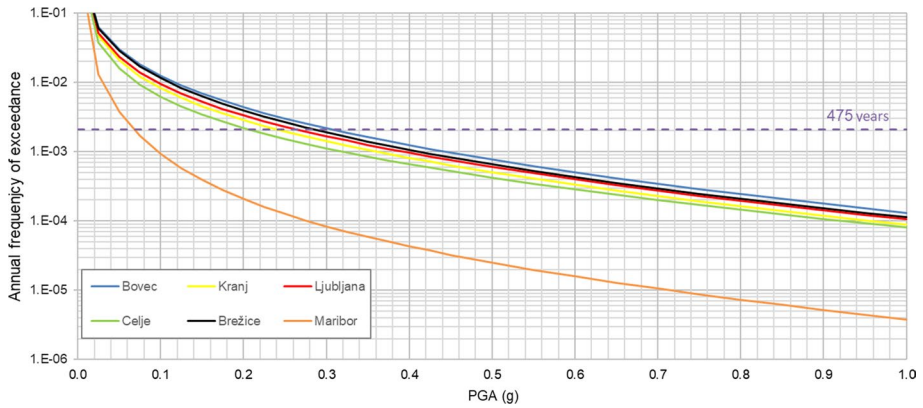
Fig. 12 Mean PGA seismic hazard curves for six chosen Slovenian sites (their locations are shown in Fig. 11)
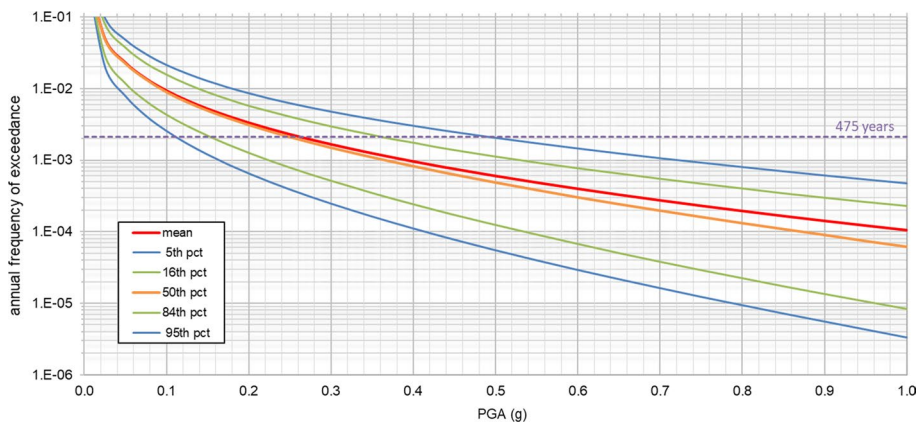
**Fig. 13** Mean and percentile PGA hazard curves for the capital city Ljubljana

buildings of special importance (e.g., schools, hospitals), and ordinary buildings for other limit states require the usage of importance factors or hazard estimates at longer return periods. As the return period is inversely proportional to the annual probability of exceedance of the reference intensity values, the hazard curves can be helpful. For illustration purposes, the mean and fractile hazard curves for the overall seismogenic source model on rock are shown for the four most populated cities and two towns in the areas of the highest hazard (Fig. 12).

On the other hand, a set of fractile hazard curves presents the center, body, and range of the considered epistemic uncertainty in the seismogenic source model and GMM. As an example, the mean, 5th, 16th, 50th, 84th, and 95th percentile PGA hazard curves are shown for the capital city Ljubljana (Fig. 13).

Sometimes, we would like to know the return period of certain PGA values for a given settlement or site (Table 3). For the capital city Ljubljana, the return period of PGA = 0.1 g is around 100 years. This PGA value roughly corresponds to the intensity VII EMS-98.

Table 3 Estimated return period (in years) for the given PGA values, for six chosen Slovenian sites

PGA (g)	Bovec	Kranj	Ljubljana	Celje	Brežice	Maribor
0.1	80	120	100	160	85	1075
0.2	230	350	300	450	260	4820
0.3	460	700	600	900	530	12,000
0.4	800	1250	1000	1500	950	23,300
0.5	1300	1975	1650	2400	1500	40,000
1	7500	11,500	10,000	12,500	9000	265,000
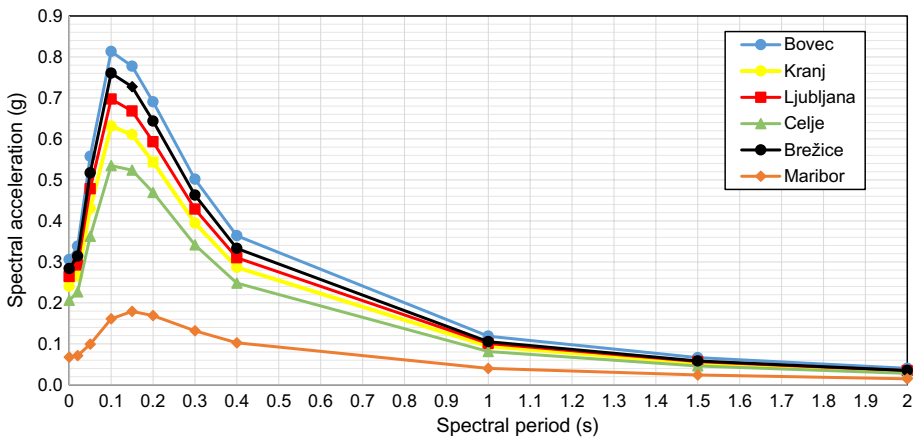
**Fig. 14** UHS for 475-year return period for six chosen Slovenian sites

The return period of PGA = 0.2 g (approximately VIII EMS-98) is around 300 years. The return period of PGA = 0.3 g is around 600 years, and the return period of PGA = 0.4 g (approximately IX EMS-98) would be roughly around 1000 years.

3.4 Spectral acceleration hazard maps and UHS

Besides the PGA maps, we have calculated the mean SA maps for ten spectral periods (0.02, 0.05, 0.1, 0.15, 0.2, 0.3, 0.4, 1, 1.5, and 2 s), and the mean UHS for 23 selected locations. For illustration purposes, UHS for the 475-year return period for six Slovenian settlements are shown in Fig. 14.

In the forthcoming EC8, PGA will no longer be the fundamental ground motion parameter, on which all other design ground motion parameters are based. Instead, of special importance will be two parameters of the horizontal 5% damped elastic response spectrum: $S_{\alpha,475}$, maximum response SA, corresponding to the constant acceleration range, and $S_{\beta,475}$, SA at the vibration period 1,0 s (CEN 2021). The forthcoming EC8 defines two options for deriving $S_{\beta,475}$: using a prescribed ratio with $S_{\alpha,475}$, or with a direct calculation from a seismic hazard model.

The values of $S_{\alpha,475}$ (plateau of the spectrum) could be estimated with the SA that gives the largest value, or with a weighted average of SA values near the maximum. In our case, the maximum SA values are obtained at the vibration period of 0.1 s for the majority of
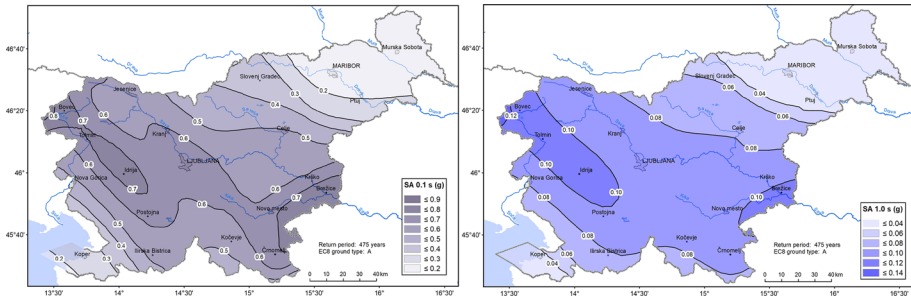
Fig. 15 Left: mean SA (0.1 s), right: mean SA (1.0 s) seismic hazard maps, both for 475 year return period and on rock (Vs30 = 800 m/s)

Table 4 Average PGA values inside Slovenia obtained from the overall seismogenic source model logic tree, four individual seismogenic source models, and the separate parts of the F + B model

Seismogenic source model	Overall	A	P	F + A	F + P	F only	B (A) only	B (P) only
Average PGA (g)	0.186	0.183	0.178	0.198	0.2	0.098	0.15	0.152

Slovenian sites. One of the options for obtaining parameters $S_{\alpha,475}$ and $S_{\beta,475}$ on ground type A for 475-year return period is presented in Fig. 15: mean SA (0.1 s), and SA (1.0 s) seismic hazard maps, respectively.

4 Discussion and conclusions

4.1 Comparison of PGA maps from individual seismogenic source models

Figures 7, 8, and 9 show which parts of Slovenia are most influenced by the individual seismogenic source model. The area seismogenic source model emphasizes the SE part of Slovenia (around Brežice and Črnomelj), as the Gorjanci area source has the largest seismic activity (the largest number of earthquakes per unit area).

The contribution of the P model consists of two parts: the density of earthquakes from the complete catalog again exposes SE Slovenia, while the energy-based model points out the area of the strongest earthquakes (Friuli and Dinarides) and consequently emphasizes the hazard in the NW of Slovenia. The contribution of the fault model is clearly correlated with the most active faults of the Dinaric system.

The comparison of an average PGA among the overall model, four individual seismogenic source models, as well as for the two parts of the F + B models, is shown in Table 4. As can be seen, the four seismogenic source models are quite balanced, with the largest difference of 11%, obtained between the largest contribution from the F + P model, and the smallest from the P model.

The two parts of the F + B model are less balanced, but still, the hazard results are not driven either by seismogenic faults alone or by background alone. Considering the

Table 5 Mean, standard deviation, and percentile PGA values in Slovenia

Mean, standard deviation, or percentile	Mean	SD	5	16	50	84	95
Average PGA (g)	0.186	0.136	0.076	0.104	0.167	0.254	0.334
max PGA (g)	0.323	0.327	0.137	0.201	0.270	0.469	0.524
Average percentile to mean ratio			0.41	0.56	0.90	1.37	1.80

appropriate magnitude range, the background sources produce larger ground motions than the fault sources.

4.2 Range of epistemic uncertainty in overall hazard values

The mean PGA values (Fig. 9, left) range up to 0.323 g, while the largest median values are up to 0.270 g (Fig. 9, right). The range of epistemic uncertainty is very large and is expressed in Table 5 in terms of average, maximum, and average percentile to mean ratio.

For the capital city Ljubljana, the mean value for the 475-year return period is 0.259 g (with a standard deviation of 0.173 g). The median value is 0.248 g, the difference between the 5th and 95th percentile is around 0.4 g and the range is between 0.1 g and 0.5 g (Fig. 13).

4.3 Comparison between UHS plateau and PGA values

For the majority of Slovenian sites, the spectra reach a peak value at SA (0.1 s). For the sites with PGA below 0.2 g, the values of SA (0.1 s) and SA (0.15 s) are almost equal, while for the sites with PGA < 0.1 g, the peak value is reached at SA (0.15 s). This is partly visible in Fig. 14. For design purposes, all PGA values below 0.1 g will be rounded up, so we can assume that SA (0.1 s) is a good approximation of plateau for all locations inside Slovenia. According to the current EC8, the value on the spectrum plateau should equal 2.5 PGA. The comparison among 2.5 PGA (plateau), SA (0.1 s), and SA (0.15 s) for the six chosen settlements is shown in Table 6. We can see that both, SA (0.1 s) and SA (0.15 s) approximate the plateau values quite well.

Considering all Slovenian sites, the average ratio between SA (0.1 s) and PGA is 2.55 (from 2.31 to 2.68), and the average ratio between SA (0.15 s) and PGA is 2.57 (from 2.50 to 2.73). However, both ratios are affected by sites of very low PGA values.

4.4 Highlights and features of the SHMS21 model

To conclude, we would like to summarize the main highlights of the new seismic hazard model for Slovenia. In comparison to the previous hazard model from 2001, we first updated the earthquake catalog to contain recent instrumental earthquakes and revised historical earthquakes; this homogenous earthquake catalog was updated and harmonized with the neighboring areas.

Further, we established a novel database of active seismogenic faults, together with fault parametrization. State-of-practice seismogenic source models of area, gridded, and

Table 6 SA values for the selected Slovenian sites, and PGA comparison with plateau values

SA vibration period (s)	Bovec	Kranj	Ljubljana	Celje	Brežice	Maribor
0	0.305	0.241	0.264	0.206	0.284	0.067
0.02	0.338	0.265	0.292	0.227	0.314	0.071
0.05	0.557	0.431	0.478	0.363	0.517	0.099
0.1	0.813	0.631	0.697	0.535	0.760	0.161
0.15	0.777	0.610	0.668	0.524	0.727	0.179
0.2	0.690	0.544	0.593	0.469	0.644	0.169
0.3	0.502	0.395	0.429	0.341	0.463	0.132
0.4	0.364	0.287	0.310	0.248	0.333	0.103
1	0.119	0.094	0.101	0.081	0.105	0.040
1.5	0.066	0.053	0.057	0.046	0.058	0.024
2	0.040	0.032	0.034	0.028	0.035	0.015
plateau: 2.5 PGA	0.764	0.602	0.660	0.516	0.709	0.168
SA(0.1 s)−2.5 PGA	0.050	0.030	0.037	0.019	0.051	-0.007
SA(0.1 s)/PGA	2.662	2.623	2.640	2.594	2.680	2.392
SA(0.15 s)/PGA	2.545	2.537	2.529	2.539	2.564	2.664

fault-specific seismogenic sources were ensembled to capture the spatial and temporal variability of the earthquake recurrence rates within the region.

We used a state-of-art regionally adapted backbone ground motion model, and a balanced logic tree to capture inherent epistemic uncertainty of data quality, methods, and model building assumptions. A seismic hazard was estimated in a mode compatible with the European seismic hazard community and services (EFEHR 2022), including the OpenQuake (Pagani et al 2014), which enables standardized input and output files.

Declarations

Competing interest The authors have no relevant financial or non-financial interests to disclose.

Conflict of interest The authors declare that they have no conflicts of interest.

References

Aki K (1965) Maximum likelihood estimate of b in the formula log (N) = a − bM and its confidence limits. Bull Earthq Res 43:237–239

Akkar S, Bommer JJ (2010) Empirical equations for the prediction of PGA, PGV and spectral accelerations in Europe, the Mediterranean region and the Middle East. Seismol Res Lett 81(2):195–206

Akkar S, Sandıkkaya MA, Ay BÖ (2014a) Compatible ground motion prediction equations for damping scaling factors and vertical-to-horizontal spectral amplitude ratios for the broader Europe region. Bull Earthq Eng 12:517–547. https://doi.org/10.1007/s10518-013-9537-1

Akkar S, Sandıkkaya MA, Bommer JJ (2014b) Empirical ground-motion models for point and extended-source crustal earthquake scenarios in Europe and the Middle East. Bull Earthq Eng 12(1):359–387. https://doi.org/10.1007/s10518-013-9461-4

Ameri G, Baumont D, Gomes C, Martin C, Secanell R, Le Dortz K, Le Goff B (2015) On the choice of maximum earthquake magnitude for seismic hazard assessment in metropolitan France—insight from the Bayesian approach, 9e`me Colloque National AFPS, 30/11–02/12. Marne-la-Valle´e

ARSO (2001) Design ground acceleration map of Slovenia. Slovenian Environment Agency (ARSO), Ljubljana.   http://www.arso.gov.si/potresi/potresna%20nevarnost/projektni_pospesek_tal.html. Accessed 17 Nov 2021

Atanackov J, Jamšek Rupnik P, Jež J, Celarc B, Novak M, Milanič B, Markelj A, Bavec M, Kastelic V (2021a) Database of active faults in slovenia: compiling a new active fault database at the junction between the alps, the Dinarides and the Pannonian basin tectonic Domains. Front Earth Sci. https://doi.org/10.3389/feart.2021.604388

Atanackov J, Jamšek Rupnik P, Celarc B, Jež J, Novak M, Milanič B, Markelj A (2021b) Tolmač potresnih virov in ocenjevanje geološko določenih parametrov za karto potresne nevarnosti Slovenije (Explanatory text of fault seismic sources and estimation of geologically determined parameters for Slovenian seismic hazard map). Geological Survey of Slovenia, Ljubljana, p 139 (in Slovene)

Atanackov J, Jamšek Rupnik P, Zupančič P, Šket Motnikar B, Živčić M, Čarman M, Milanič B, Kastelic V, Rajh G, Gosar A (2022) Seismogenic fault and area sources for probabilistic seismic hazard model in Slovenia. PANGAEA. https://doi.pangaea.de/10.1594/PANGAEA.940100

Basili R, Kastelic V, Demircioglu MB, Garcia Moreno D, Nemser ES, Petricca P, Sboras SP, Besana-Ostman GM, Cabral J, Camelbeeck T, Caputo R, Danciu L, Domac H, Fonseca J, García-Mayordomo J, Giardini D, Glavatovic B, Gulen L, Ince Y, Pavlides S, Sesetyan K, Tarabusi G, Tiberti MM, Utkucu M, Valensise G, Vanneste K, Vilanova S, Wössner J (2013) The European database of seismogenic faults (EDSF) compiled in the framework of the Project SHARE. https://doi.org/10.6092/INGV.IT-SHARE-EDSF

Bindi D, Pacor F, Sabetta F, Massa M (2009) Towards a new reference ground motion prediction equation for Italy: update of the Sabetta-Pugliese (1996). Bull Earthq Eng 7:591–608. https://doi.org/10.1007/s10518-009-9107-8

Bindi D, Massa M, Luzi L, Ameri G, Pacor F, Puglia R, Augliera P (2014) Pan-European ground-motion prediction equations for the average horizontal component of PGA, PGV, and 5%-damped PSA at spectral periods up to 3s using the RESORCE dataset. Bull Earthq Eng 12(1):391–430. https://doi.org/10.1007/s10518-013-9525-5

Bindi D, Cotton F, Kotha SR, Bosse C, Stromeyer D, Grünthal G (2017) Application-driven ground motion prediction equation for seismic hazard assessments in non-cratonic moderate-seismicity areas. J Seismol 21:1201–1218. https://doi.org/10.1007/s10950-017-9661-5

Bommer JJ, Crowley H (2017) The purpose and definition of the minimum magnitude limit in PSHA calculations. Seismol Res Lett 88:1097–1106

BSHAP, Harmonization of seismic hazard maps for the western Balkan countries (2011) NATO SfP Project No. 983054. http://www.seismo.co.me/documents/NATO%20SfP%20No.983054%20FINAL%20REPORT.pdf Accessed 14 Feb 2022

Camassi R, Caracciolo CH, Castelli V, Slejko D (2011) The 1511 Eastern Alps earthquakes: a critical update and comparison of existing macroseismic datasets. J Seismol 15:191–213

Caracciolo CH, Slejko D, Camassi R, Castelli V (2021) The eastern Alps earthquake of 25 January 1348: new insights from old sources. Bull Geophys Oceanogr 62(3):335–364. http://www3.inogs.it/bgo/pdf/bgo00364_Caracciolo.pdf. Accessed 14 Feb 2022

Carafa M, Valensise G, Bird P (2017) Assessing the seismic coupling of shallow continental faults and its impact on seismic hazard estimates: a case-study from Italy. Geophys J Int 209:32–47. https://doi.org/10.1093/gji/ggx002

CEN (2004) European Committee for Standardization, EN 1998–1:2004 Eurocode 8: Design of structures for earthquake resistance. Part 1: General rules, Seismic actions and rules for buildings. https://www.phd.eng.br/wp-content/uploads/2015/02/en.1998.1.2004.pdf. Accessed 17 Nov 2021

CEN (2021) Eurocode 8: Earthquake resistance design of structures, EN1998–1–1_version_01–10–2021, Working draft

Chiou B, Youngs R (2014) Update of the Chiou and Youngs NGA model for the average horizontal component of peak ground motion and response spectra. Earthq Spectra 30(3):1117–1153. https://doi.org/10.1193/072813EQS219M

Cornell CA (1968) Engineering seismic risk analysis. Bull Seismol Soc Am 58:1583–1606

Cornell CA, Vanmarcke EH (1969) The major influences on seismic risk. In Proceedings of the fourth world conference on earthquake engineering, Santiago, Chile

Danciu L, Giardini D (2015) Global Seismic Hazard Assessment Program - GSHAP legacy. Ann Geophys 58(1). https://www.annalsofgeophysics.eu/index.php/annals/article/view/6734. Accessed 18 Nov 2021

Danciu L, Nandan S, Reyes C, Basili R, Weatherill G, Beauval C, Rovida A, Vilanova S, Sesetyan K, Bard P-Y, Cotton F, Wiemer S, Giardini D (2021) The 2020 update of the European Seismic Hazard Model: Model Overview. EFEHR Technical Report 001, v1.0.0. https://gitlab.seismo.ethz.ch/efehr/eshm20/-/tree/master/documentation. Accessed 11 Feb 2021. https://doi.org/10.12686/a15

DISS Working Group (2018) Database of Individual Seismogenic Sources (DISS), Version 3.2.1: a compilation of potential sources for earthquakes larger than M 5.5 in Italy and surrounding areas. Istituto Nazionale di Geofisica e Vulcanologia. http://diss.rm.ingv.it/diss/. Accessed 17 Nov 2021. https://doi.org/10.6092/INGV.IT-DISS3.2.1

Douglas J (2018) Calibrating the backbone approach for the development of earthquake ground motion models. In: Best practice in physics-based fault rupture models for seismic hazard assessment of nuclear installations: issues and challenges towards full seismic risk analysis, Cadarache, France. https://strathprints.strath.ac.uk/63991/1/Douglas_PSHANI_2018_Calibrating_the_backbone_approach_for_the_development_of_earthquake_ground_motion_models.pdf. Accessed 17 Nov 2021

Douglas J (2021) Ground motion prediction equations 1964–2020, Department of Civil and Environmental Engineering University of Strathclyde. http://www.gmpe.org.uk/gmpereport2014.html. Accessed 17 Nov 2021

EFEHR (2022) European facilities for earthquake hazard and risk service. http://www.efehr.org. Accessed 14 Feb 2022

Finetti I, Russi M, Slejko D (1979) The Friuli earthquake (1976–1977). Tectonophys 53:261–272

Frankel AD (1995) Mapping seismic hazard in the Central and Eastern United States. Seismol Res Lett 66(4):8–21

Gardner JK, Knopoff L (1974) Is the sequence of earthquakes in Southern California, with aftershocks removed, Poissonian? Bull Seismol Soc Am 64:1363–1367

Gentili S, Sugan M, Peruzza L, Schorlemmer D (2011) probabilistic completeness assessment of the past 30 years of seismic monitoring in northeastern Italy. Phys Earth Planet Inter 186(1–2):81–96. https://doi.org/10.1016/j.pepi.2011.03.005

GeoRisk (1995–2019) Hungarian earthquake bulletin, Hungarian Academy of Sciences. Geodetic and Geophysical Research Institute, Seismological Observatory, Budapest. https://www.georisk.hu/Bulletin/bulletine.html. Accessed 17 Nov 2021

GFZ (2008) Croatian earthquake catalogue (computer file). Faculty of Science, University of Zagreb, Zagreb, Department of Geophysics

Giardini D, Woessner J, Danciu L (2014) Mapping Europe's Seismic Hazard. Eos 95(29):261–262. https://doi.org/10.1002/2014EO290001

Godano C, Pingue F (2000) Is the seismic moment – frequency relation universal? Geophys J Int 142:193–198

Grünthal G (1998) European Macroseismic Scale. Cahiers du Centre Europeen de Geodynamique et de Seismologie. https://doi.org/10.2312/EMS-98.full.en

Grünthal G, Wahlström R, Stromeyer D (2009) The unified catalogue of earthquakes in central, north-
ern, and Northwestern Europe (CENEC)—updated and expanded to the last millennium. J Seismol
13:517–541. https://doi.org/10.1007/s10950-008-9144-9

Hale C, Abrahamson N, Bozorgnia Y (2018) Probabilistic seismic hazard analysis code verification,
PEER report 2018/03. https://peer.berkeley.edu/sites/default/files/2018_03_hale_final_8.13.18.pdf.
Accessed 17 Nov 2021

Hanks TC, Bakun WH (2002) A bilinear source-scaling model for M–log A observations of continental
earthquakes. Bull Seismol Soc Am 92(5):1841–1846

Herak D (1995) Razdioba brzina prostornih valova potresa i seizmičnost širega područja Dinare (Distribu-
tion of body-wave velocities and seismicity of the greater Dinara Mt. Region). Ph. D. Dissertation,
University of Zagreb, Croatia (in Croatian with English abstract)

INGV (2021) Regional Centroid Moment Tensor. http://www.bo.ingv.it/RCMT/. Accessed 17 Nov 2021

INOGS - Instituto Nacionale di Oceanografia e di Geofisica Sperimentale, Centro Ricerche Sismologiche
(CRS), 1977–2019. Bollettino della Rete Sismometrica del Friuli-Venezia-Giulia. http://www.crs.
inogs.it/bollettino/RSFVG/. Accessed 17 Nov 2021

ISC—International Seismological Center (2021) ISC catalogue. http://www.isc.ac.uk/iscbulletin/search/
catalogue/. Accessed 17 Nov 2021

Johnston AC, Coppersmith K, Kanter L, Cornell C (1994) The earthquakes of stable continental regions.
Assessment of large earthquake potential. EPRI Report Tr-102261-V1, 2–1–98., Palo Alto, California

Kagan YY (1999) Universality of the seismic moment-frequency relation. Pure Appl Geophys 155:537–573

Karník V (1971) Seismicity of the European Area, Part 2. Czechoslovak Academy of Sciences, Praha

Kijko A (2012) On Bayesian procedure for maximum earthquake magnitude estimation. Res Geoph 2(1).
https://doi.org/10.4081/rg.2012.e7

Košir M, Cecić I (2011) Potres 26. marca 1511 v luči novih raziskav (The earthquake on 26 March 1511—
interpretation of some unknown historical sources). Idrijski razgledi 56(1):90–104 (in Slovene with
English abstract)

Kotha SR, Weatherill G, Bindi D et al (2020) A regionally-adaptable ground-motion model for shal-
low crustal earthquakes in Europe. Bull Earthq Eng 18:4091–4125. https://doi.org/10.1007/
s10518-020-00869-1

Lapajne JK (2000) Some features of the spatially smoothed seismicity approach. In: Lapajne JK (ed) Seis-
micity modeling in seismic hazard mapping, Workshop proceedings, Geophysical Survey of Slovenia,
Ljubljana, 27–33

Lapajne JK, Šket Motnikar B, Zabukovec B, Zupančič P (1997) Spatially-smoothed seismicity modelling of
seismic hazard in Slovenia. J Seismol 1:73–85

Lapajne JK, Šket Motnikar B, Zupančič P (2003) Probabilistic seismic hazard assessment methodology for
distributed seismicity. Bull Seismol Soc Am 93(6):2502–2515. https://doi.org/10.1785/0120020182

Leonard M (2010) Earthquake fault scaling: self-consistent relating of rupture length, width, average dis-
placement, and moment release. Bull Seismol Soc Am 100(5A):1971–1988. https://doi.org/10.1785/
0120090189

Markušić S, Gülerce Z, Kuka N et al (2016) An updated and unified earthquake catalogue for the Western
Balkan Region. Bull Earthq Eng 14:321–343. https://doi.org/10.1007/s10518-015-9833-z

Miller AC, Rice TR (1983) Discrete approximations of probability distributions. Manag Sci 29(3):352–362

Monelli D, Pagani M, Weatherill G, Danciu L, Garcia J (2014) Modeling distributed seismicity for probabil-
istic seismic-hazard analysis: implementation and insights with the OpenQuake engine. Bull Seismol
Soc Am 104(4):1636–1649. https://doi.org/10.1785/0120130309

NEIC—National Earthquake Information Center/USGS (2015) World Data Center for Seismology, Catalog
of earthquakes located by the USGS/NEIC (1973 - present), Denver. http://earthquake.usgs.gov/earth
quakes/search/. Accessed 17 Nov 2021

OpenQuake (2021) OpenQuake engine opensource application. https://github.com/gem/oq-engine.
Accessed 17 Nov 2021

Pagani M, Monelli D, Weatherill G, Danciu L, Crowley H, Silva V, Henshaw P, Butler L, Nastasi M, Panz-
eri L, Simionato M, Vigano D (2014) OpenQuake engine: an open hazard (and risk) software for the
global earthquake model. Seismol Res Lett 85:692–702. https://doi.org/10.1785/0220130087

Plešinger A, Kozák J (2003) Beginnings of regular seismic service and research in the Austro-Hungarian
Monarchy: Part II. Stud Geophys Geod 47:757−791

Poli ME, Zanferrari A (2018) The seismogenic sources of the 1976 Friuli earthquakes: a new seismotec-
tonic model for the Friuli area. Boll. Geof Teor Appl 59(4):463–480

Poli ME, Peruzza L, Rebez A, Renner G, Slejko D, Zanferrari A (2002) New seismotectonic evidence from
the analysis of the 1976–1977 and 1977–1999 seismicity in Friuli (NE Italy). Boll Geof Teor Appl
43(1–2):53–78

Poljak M, Živčić M, Zupančič P (2000) Seismotectonic characteristics of Slovenia. Pure Appl Geoph 157:37–55

PVL—Potresi v letu (1994–2019) Annual bulletins, Slovenian Environment Agency (ARSO), Seismology Office, Ljubljana (in Slovene with English abstract)

Reiter L (1990) Earthquake hazard analysis, Issues and Insights. Columbia University Press, New York, p 254

Ribarič V (1982) Seismicity of Slovenia—catalogue of earthquakes (792 A.D. - 1981). Ljubljana, p 650

Sabetta F, Pugliese A (1996) Estimation of response spectra and simulation of nonstationary earthquake ground motions. Bull Seismol Soc Am 86:337–352

Schmid SM, Fügenschuh B, Kounov A, Matenco L, Nievergelt P, Oberhänsli R, Pleuger J, Schefer S, Schuster R, Tomljenović B, Ustaszewski K, van Hinsbergen DJJ (2020) Tectonic units of the Alpine collision zone between Eastern Alps and western Turkey. Gondwana Res 78:308–374. https://doi.org/10.1016/j.gr.2019.07.005

Scordilis EM (2006) Empirical global relations converting MS and mb to moment magnitude. J Seismol 10:225–236. https://doi.org/10.1007/s10950-006-9012-4

Shebalin NV, Karník V, Hadžievski D (eds) (1974) Catalogue of earthquakes. Part I 1901–1970; Part II prior to 1901. UNDP/UNESCO Survey of the Seismicity of the Balkan Region. Skopje, pp 1–65 and App

Šket Motnikar B (2010) Preverjanje karte potresne nevarnosti Slovenije (Reestimation of Slovenian seismic hazard map), Potresi v letu 2009 113–127, Slovenian Environment Agency (ARSO), Ljubljana. http://www.arso.gov.si/potresi/poro%C4%8Dila%20in%20publikacije/Potresi%20v%20letu%202009_int.pdf. Accessed 17 November 2021 (in Slovene with English abstract)

Šket Motnikar B, Lapajne JK, Zupančič P, Zabukovec B (2000) Application of the spatially smoothed seismicity approach for Slovenia. In: Lapajne JK (ed) Seismicity modeling in seismic hazard mapping, Workshop proceedings, Geophysical Survey of Slovenia, 125–133

Šket Motnikar B, Čarman M, Godec M, Zupančič P, Cecić I (2016) Potres 1. novembra 2015 na Gorjancih (The Earthquake of 1 November 2015 at Gorjanci Mountains). Ujma 30: 61–68 (in Slovene with English abstract)

Stucchi M, Rovida A, Gomez Capera AA, Alexandre P, Camelbeeck T, Demircioglu MB, Gasperini P, Kouskouna V, Musson RMW, Radulian M, Sesetyan K, Vilanova S, Baumont D, Bungum H, Fäh D, Lenhardt W, Makropoulos K, Martinez Solares JM, Scotti O, Živčić M, Albini P, Batllo J, Papaioannou C, Tatevossian R, Locati M, Meletti C, Viganò D, Giardini D (2013) The SHARE European earthquake catalogue (SHEEC) 1000–1899. J Seismol 17:523–544. https://doi.org/10.1007/s10950-012-9335-2

Tertulliani A, Cecić I, Meurers R, Sović I, Kaiser D, Grunthal G, Pazdirkova J, Sira C, Guterch B, Kysel R, Camelbeeck T, Lecocq T, Szany G (2018) The 6 May 1976 Friuli earthquake: re-evaluating and consolidating transnational macroseismic data. Boll Geof Teor Appl 59(4):417–444.

USGS (2021) Search Earthquake Catalog. https://earthquake.usgs.gov/earthquakes/search/. Accessed 17 Nov 2021

Utsu T (2002) Relationships between Magnitude Scales. IASPEI Handbook Chapter 44:773–746

Ward SN (1998) On the consistency of earthquake moment release and space geodetic strain rates: Europe. Geophys J 135(3):1011–1018. https://doi.org/10.1046/j.1365-246X.1998.t01-2-00658.x

Weatherill G, Kotha SR, Cotton F (2020) A regionally-adaptable "scaled backbone" ground motion logic tree for shallow seismicity in Europe: application to the 2020 European seismic hazard model. Bull Earthq Eng 18:5087–5117. https://doi.org/10.1007/s10518-020-00899-9

Wells DL, Coppersmith KL (1994) New empirical relationship among magnitude, rupture length, rupture width, rupture area, and surface displacement. Bull Seismol Soc Am 84(4):974–1002

Wiemer S, Danciu L, Edwards B, Marti B, Fäh D, Hiemer S, Wössner J, Cauzzi C, Kästli P, Kremer K (2016) Seismic hazard model 2015 for Switzerland (SUIhaz2015), Report Swiss Seismological Service (SED) at ETH Zurich. http://www.seismo.ethz.ch/export/sites/sedsite/knowledge/.galleries/pdf_knowledge/SUIhaz2015_final-report_16072016.pdf_2063069169.pdf. Accessed 17 Nov 2021

Woessner J, Danciu L, Giardini D, Crowley H, Cotton F, Grünthal G, Valensise G, Arvidsson R, Basili R, Demircioglu MN, Hiemer S, Meletti C, Musson RW, Rovida AN, Sesetyan K, Stucchi M, the SHARE consortium, (2015) The 2013 European seismic hazard model: key components and results. Bull Earthq Eng 13:3553–3596. https://doi.org/10.1007/s10518-015-9795-1

Youngs RR, Coppersmith KJ (1985) Implications of fault slip rates and earthquake recurrence models to probabilistic seismic hazard estimates. Bull Seismol Soc Am 75:939–964

Zabukovec B (2000) OHAZ—a computer program for spatially smoothed seismicity approach. In: Lapajne JK (ed) Seismicity modeling in seismic hazard mapping, Workshop proceedings, Ministry

of the Environment and Spatial Planning, Geophysical Survey of Slovenia, Ljubljana, Slovenia, 135–140.

ZAMG (1998–2013) Zentralstalt Für Meteorologie und Geodynamik, Erdbeben-Jahresberichte. http://www.zamg.ac.at/cms/de/geophysik/erdbeben/erdbebenarchiv/jahresberichte. Accessed 17 Nov 2021

ZAMG (2002) Austrian earthquake catalog (computer file). Central Institute of Meteorology and Geodynamics, Vienna

ZAMG (2006–2014) Austrian Bulletin of Regional and Teleseismic events recorded with ZAMG-Stations in Austria (Computer file), Central Institute of Meteorology and Geodynamics, Vienna

Živčić M (1994) Earthquake Catalog. In: Fajfar P, Lapajne J (eds) Probabilistic Assessment of Seismic Hazard at Krško Nuclear Power Plant, Rev.1, University of Ljubljana, Department of Civil Engineering

Živčić M (2004) Earthquake Catalog. In: Fajfar P (ed) Revised PSHA for NPP Krško site, PSR-NEK-2.7.2, Revision 1, Ljubljana

Živčić M, Cecić I, Čarman M, Jesenko T, Ložar Stopar M, Pahor J (2010) Earthquake catalog rev. 2, Slovenian Environment Agency (ARSO), Seismology and geology office, Ljubljana

Živčić M, Cecić I, Čarman M, Jesenko T, Ložar Stopar M, Pahor J (2015) Earthquake catalog NEK2015 of Slovenia and the Region, Final Report, Slovenian Environment Agency (ARSO), Seismology and geology office, Ljubljana

Živčić M, Cecić I, Čarman M, Jesenko T, Ložar Stopar M, Pahor J (2018) Earthquake catalog KPN2018 of Slovenia and surrounding, rev. 3, Slovenian Environment Agency (ARSO), Seismology and geology office, Ljubljana

Zsíros T, Mónus P, Tóth L (1988) Hungarian earthquake catalog (456–1986), Seismological Observatory, Geodetic and Geophysical Research Institute. Hungarian Academy of Sciences, Budapest, p 182, Computer file (1991) - data from 456 to 1991